

Nanocrystal-matrix interaction in mixtures of KCN+KI investigated by x-ray diffraction

H.-J. Weber,¹ H. L. Keller,² M. Paulus,³ and C. Sternemann³¹*Institut für Physik, Universität Dortmund, D-44221 Dortmund, Germany*²*Fachbereich Chemie, Universität Dortmund, D-44221 Dortmund, Germany*³*Institut für Physik, DELTA, Universität Dortmund, D-44221 Dortmund, Germany*

(Received 20 December 2004; revised manuscript received 11 April 2005; published 15 July 2005)

Powder x-ray diffraction has been used to search for effects that indicate the influence of ionic KCN nanocrystals embedded in the ionic compound KI by measuring Bragg reflections of the matrix. Due to the extremely slow phase separation processes on the time scale of months it was necessary to perform measurements in several periods. At first the boundary between solid solutions of KCN in KI and the mixture of the two crystalline compounds has been determined. Finally, a splitting of diffraction peaks has been observed in a powder sample made from an optically homogeneous large single crystal containing a small excess of KCN. The splitting is traced back to elastic forces acting at the interface between embedded KCN-rich nanocrystals and the surrounding matrix. In contrast to piezoelectric nanocrystals the elastic continuum theory is working quantitatively in the ionic system KCN—KI.

DOI: 10.1103/PhysRevB.72.045432

PACS number(s): 61.10.Nz, 61.46.+w, 62.25.+g

I. INTRODUCTION

Studies of nanocrystals are usually focused on metals and semiconductors.^{1,2} Whereas in the past preparation techniques,¹ nucleation phenomena, and new properties related to quantum-confinement effects² were the main subjects of scientific research, in the last few years x-ray diffraction techniques have been developed to detect structural details. Examples are the determination of surface stresses in Cu (Ref. 3) and InAs/GaAs (Ref. 4) nanocrystals by grazing incidence x-ray scattering, of strain and composite profiles in SiGe islands by anomalous x-ray scattering,⁵ and of chemical gradients in Ge domes grown on Si by a combination of both methods, called grazing incidence anomalous scattering.⁶ A combination of anomalous diffraction and EXAFS was used to characterize Ge nanocrystals embedded in amorphous Ge.⁷ Samples of dense accumulations of nanocrystals made from Pd,⁸ Si,⁹ C,¹⁰ and SiC (Ref. 11) have been studied by powder diffraction combined with a special model of data analysis,⁸ with oxidation of grain surfaces,⁹ and with a crystallographic core-shell model of nanocrystals which includes measurements for an extended range of the scattering vector.^{10,11}

In spite of the large amount of ionic compounds, only some nanocrystalline oxides with significant ionicity have been investigated in the past.¹² This was done mainly in order to optimize physical properties related to ferroelectricity.¹³ Independent of the type of bonding, each nanocrystal needs a connection to its environment. Most generally, such connections are described in terms of elastic forces, where the nature of these forces depends on the type of bonding in both materials, the nanocrystal and the matrix. This view stresses the importance of investigating ionic compounds due to the fundamental role of Coulomb forces in solid materials. Recently the strain induced by CuCl nanocrystals in a single crystal of NaCl was observed by sensitive elastic measurements.¹⁴ The strain was found to be two orders of magnitude larger than predicted by the elastic continuum theory. An explanation could be an electromechanical

coupling between CuCl and NaCl.¹⁴ This idea motivated us to consider a similar system in which not only the matrix but also the nanocrystal is an ionic compound without any piezoelectricity.

Alkali-halides are prototypes of ionic compounds. For a particular reason we use for an experimental study KCN embedded in KI. The CN⁻ ion behaves as an elastic dipole at room temperature and one expects that in this case elastic interactions are well developed in a heterogeneous material. Therefore, (KCN)_x(KI)_{1-x}, where x denotes the molar fraction of KCN, seems to be an ideal material to decide whether the standard treatment of nanocrystal-matrix interaction on basis of the elastic continuum theory works quantitatively or only approximately. This is the main aim of the present work.

KCN and KI crystallize both in the sodium-chloride structure but the lattice parameter of KCN ($a_{\text{KCN}}=6.523 \text{ \AA}$) is remarkable smaller than that of KI ($a_{\text{KI}}=7.0655 \text{ \AA}$).¹⁵ Therefore, at ambient conditions the equilibrium state of mixed materials is the existence of two phases if the composition is not too close to one of the pure compounds. In contrast to the equilibrium conditions, the solidification of a melt (KCN)_x(KI)_{1-x} by use of the Czochralski technique results in as-grown crystals of optical homogeneity for all x . Experience shows that large crystals (volume several cm³) remain optically clear at ambient conditions for two months and more.¹⁶ The extremely long time single crystals need to reach thermodynamic equilibrium is understandable because the separation into two phases depends on the diffusion of the big anions CN⁻ (radius $\approx 1.88 \text{ \AA}$) and I⁻ (radius $\approx 2.2 \text{ \AA}$).¹⁷ These conditions make the determination of the boundaries difficult which exist between homogeneous solid solutions and the heterogeneous field of two phases. Near to each of the two boundaries with $0 < x_{\text{ss}}^a < 0.1$ or $1 > x_{\text{ss}}^b > 0.9$ the concentration of the minor component in the two-phase mixture is small. Such samples can be used to study nucleation and the forces acting between small grains and the surrounding matrix independently from mutual interactions

between grains which renders a theoretical analysis of internal stresses more easy and more safety than in the case of dense structures of nanocrystals. But, the same conditions which make compositions near x_{ss}^a or x_{ss}^b interesting prevent the detection of seeds by x-ray diffraction.

At least in the first step of a phase separation process the common cation sublattices of the matrix and of the seed should be maintained. As a result the crystallographic orientations of both components will coincide. That this happens was demonstrated in the system CuCl-NaCl in which the anion sublattices of CuCl and NaCl are the same.¹⁸ Due to this kind of connection one has to assume that strong forces exist between seed and matrix. We estimate a possible interfacial stress of 3 GPa in the system KCN—KI caused by these forces. Such a large stress modifies the lattice parameter of the matrix. Even in the case of low concentration the modification should be detectable if diffraction is performed with good resolution.

In the case of nanocrystalline semiconductors exciton spectroscopy is an excellent experimental method to study nanocrystals embedded in a dielectric matrix.² We indeed have observed an excitonlike absorption peak of KI in KCN-rich samples of $(\text{KCN})_x(\text{KI})_{1-x}$.¹⁶ In principle, it should be possible to observe also exciton peaks of KCN in KI-rich samples. However, they appear at photon energies well above the gap energy of the matrix.¹⁹ Thus, optical measurements have to be performed in reflection in a vacuum apparatus. Such measurements are by no means sufficiently sensitive. In fact, it is difficult to find an appropriate experimental method which is able to prove the existence of few grains in the nanocrystalline state directly and it seems to be even more difficult to get information about their interaction with the surrounding matrix. These considerations stress the importance to develop alternative experimental methods. In the present work we use mainly powder x-ray diffraction but in contrast to the experiments reported in Refs. 3–11 we consider Bragg peaks of the matrix and not of the nanocrystals.

II. EXPERIMENTAL

Powder samples were prepared from single crystals of $(\text{KCN})_x(\text{KI})_{1-x}$ already used previously for an extensive characterization of the system.¹⁶ Due to the slow structural relaxation of the material it was desirable to check whether changes are observable several years later.

X-ray diffraction has been carried out at the beamline SAW2 (BL 9) of the Dortmund Electron Accelerator (DELTA) during two beam-time periods. The radiation supplied by the superconducting asymmetric wiggler, which has a critical energy of 7.9 keV, is monochromatized using a Si (311) double crystal monochromator which covers an energy range from 5 up to 30 keV with a photon flux of about 3×10^{10} photons \times s⁻¹ \times mm⁻² at 9 keV. The first measurements have been performed at an energy of 15.5 keV with a preliminary diffraction setup in horizontal scattering geometry. The beam size at the sample position was 1 mm horizontally and 8 mm vertically and the distance between sample and NaI detector was 830 mm. Samples have been

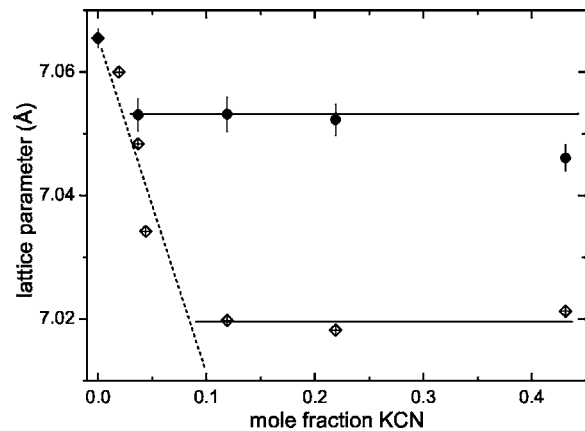


FIG. 1. Lattice parameters of $(\text{KCN})_x(\text{KI})_{1-x}$ compounds versus the mole fraction x of KCN. Diamonds represent previous data (Ref. 16). Circles are results from the first measurements at DELTA which were carried out in horizontal scattering geometry. The horizontal lines present lattice parameters of the KI-rich compound. Shifting of the line with time indicates continuation of phase separation.

filled into capillaries of 0.5 mm diameter and rotated permanently during the measurements. The overall 2Θ resolution has been estimated to be 0.053° and was dominated by the effective diameter of the capillary illuminated by the x-ray beam. The effective diameter was larger than the real one due to the sample rotation. The second measurements have been performed in vertical scattering geometry using the Huber six-circle diffractometer of the beam line SAW2. The beam size at the sample position was 2×0.7 mm² (horizontal \times vertical) and the scattered photons of 15.2 keV energy have been detected by a NaI detector at a distance of 1000 mm from the sample position. The improved overall 2Θ resolution was 0.03° . The performance of the diffractometer has been tested by recording the diffraction spectrum of α -SiO₂ in the range $10^\circ < 2\Theta < 45^\circ$. The recorded peak positions were consistent with the possible spread of lattice parameters of α -SiO₂.²⁰ This indicates that the central position of a diffraction peak can be determined with an accuracy which is better than 3×10^{-3} deg. Repeating the adjustment of a sample revealed a reproducibility of 1×10^{-3} deg.

III. RESULTS

The KI-like lattice parameters of $(\text{KCN})_x(\text{KI})_{1-x}$ samples with $x < 0.5$ are shown in Fig. 1. The present results are compared with the previous data obtained in the first year after growing the crystals.¹⁶ The dashed line in Fig. 1 shows the lattice parameters

$$a_{ss} = a_{\text{KI}} - x(a_{\text{KI}} - a_{\text{KCN}}) \quad (1)$$

of a solid solution which obeys Vegard's rule. Samples that follow Eq. (1) must be considered to be solid solutions whereas compounds on horizontal lines in Fig. 1 represent one of the two chemical components of the two-phases field of the phase diagram. The continuation of the phase separation processes in the time after the previous measurements

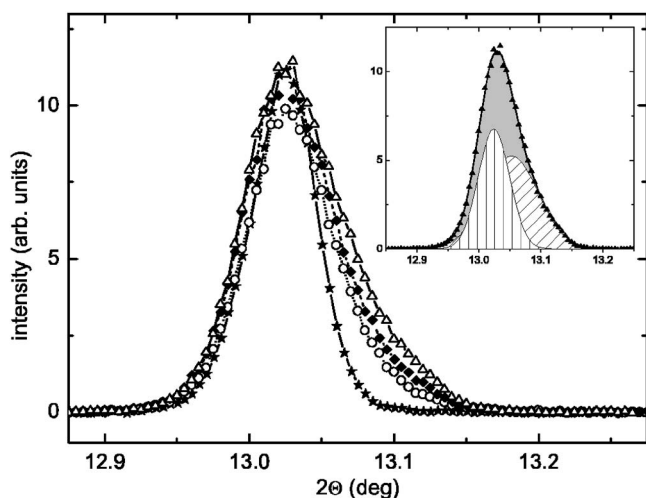


FIG. 2. Profiles of (200) reflections of $\text{KCN}_{0.038}\text{KI}_{0.962}$ (stars, solid line), $\text{KCN}_{0.12}\text{KI}_{0.88}$ (circles, dotted line), $\text{KCN}_{0.21}\text{KI}_{0.79}$ (diamonds, dashed line), and $\text{KCN}_{0.43}\text{KI}_{0.57}$ (triangles, solid line) recorded in the horizontal scattering geometry. The reflections belong to the solid circles in Fig. 1. Positions of reflections have been shifted if necessary until the maxima coincided. Notice the broadening, in particular on the right side, with increasing KCN concentration. The peak of the $x=0.43$ sample has been analyzed in the inset by assuming two Gaussian subpeaks. The more narrow one appears on the left side.

several years before is obvious because the horizontal line shifted upwards during that time. Diffraction patterns of samples with $x > 0.1$ exhibit also KCN-like diffraction peaks. The lattice parameter of the KCN-rich grains is $a=6.566 \text{ \AA}$.

It should be mentioned that samples with $x > 0.1$ are opaque because they are decomposed into small grains. Nevertheless, the original shapes of the as-grown crystals are approximately maintained and it needs some force to break the material. These observations indicate a residual intergrowth between the grains which is able to explain the decrease of lattice parameters with increasing x , in particular for $x=0.43$ (see Fig. 1). In agreement with this interpretation the diffraction peaks show an increasing linewidth with increasing x as demonstrated in Fig. 2. In addition the diffraction peaks are asymmetric for $x > 0.1$. As demonstrated in the inset of Fig. 2 with the peak of $x=0.43$, the asymmetry indicates the overlapping of two Gaussian peaks. The position of the more narrow peak on the left side agrees with the horizontal line in Fig. 1. All nine reflections between (111) and (422) of the sample with $x=0.43$ can be analyzed in a similar way as shown in Fig. 2. In all reflections the broadening appears on the right side of the curves. The fractional area of the broad band at the right side varies strongly for different crystallographic planes. The average value is 1/3 which simply indicates that about 1/3 of the surface of a KI-rich grain is connected to a KCN-rich grain. All these features indicate the intergrowth between both types of materials which results in the observed modulation of lattice parameters for $x > 0.2$.

The solid circles in Fig. 1 show that the sample with $x=0.038$ represents just the composition which is interesting for the study of effects caused by embedded nanocrystals.

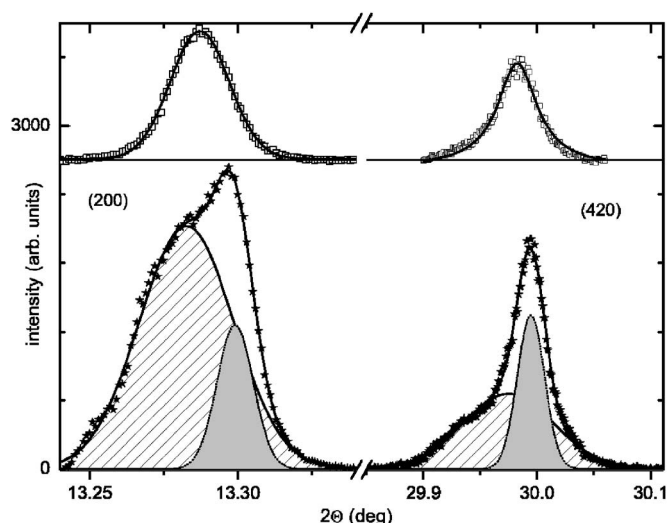


FIG. 3. Profiles of two reflections of sample S1 (stars) and sample S2 (squares). The data have been recorded in vertical scattering geometry one year after those in Fig. 2. Each reflection of sample S1 has been fitted by two Gaussian peaks. In contrast to Fig. 2, the narrow subpeak (grey background) is on the right side.

The lattice parameters of this material and of the $x=0.12$ material have been recorded again one year later utilizing a new setup with a Huber diffractometer using the vertical scattering geometry. The two samples with $x=0.038$ and $x=0.12$ will be named S1 and S2 in the following.

Results of the final measurements in the vertical scattering geometry are presented in Fig. 3 for (200) and (420) reflections. They show several remarkable features.

(i) The linewidths are smaller than in the measurements in horizontal scattering geometry which indicates that in Fig. 2 additional broadening by the apparatus is involved. This broadening was estimated from technical parameters of the two setups as $\Delta\Theta=0.044^\circ$. For a quantitative comparison we consider the linewidths of the reflections (200)-(220)-(420) observed in the horizontal (data in parentheses) and the vertical scattering geometry for sample S1:

$$0.041(0.059)-0.040(0.061)-0.044(0.069).$$

The data represent the full widths of half maximum (FWHM) in units of degrees. The different widths of both measurements are consistent with the estimated value of $\Delta\Theta$.

(ii) The reflections of sample S1 are split into a broad and a narrow peak in the measurements with vertical scattering geometry. We conclude that this splitting has become observable by the improvement of resolution. However, additional influence of final relaxation processes in the year between the two beam-time periods cannot be ruled out. The acting of such processes is more directly seen by the narrowing of the S2 peak.

(iii) S2 reflections are positioned just between the two subpeaks of S1 reflections. Within the error bars given in Fig. 1, the positions of S2 reflections did not change.

(iv) Thick samples of S1 material do not show unusual inhomogeneities under the polarizing microscope. This and the narrow reflections of S2 indicate that the splitting of S1

reflections is of different origin than the splitting shown in Fig. 2. This conclusion is supported by the result that the narrow sub-peaks are on the left side in Fig. 2 but on the right side in Fig. 3.

The lattice parameter of sample S2 is $a_{S2}=7.0507(4)$ Å. The lattice parameter of sample S1 can be obtained in two different ways.

(a) The broad subpeaks of S1 reflections are assumed to represent parts of the sample that are undistorted by nanocrystals. The corresponding parameter is $a_{S1}^{(\alpha)}=7.0525(4)$ Å. In this case the narrow subpeaks indicate an average built-in strain of $S_0^{(\alpha)}=-8.4(\pm 2.2) \times 10^{-4}$.

(b) A second averaged value is calculated by weighting the positions of each subpeak by its relative areas. The results are $a_{S1}^{(\beta)}=7.0509(4)$ Å together with the two built-in strains $S_0^{(\beta+)}=2.5 \times 10^{-4}$ and $S_0^{(\beta-)}=-5.9 \times 10^{-4}$.

IV. DISCUSSION

A. Preliminary remarks

As sample S2 is opaque, the KCN-rich grains are so large that their connections to the KI-rich matrix by a common cationic sublattice is distorted. On the other side, the KI-rich component of sample S1 shows a lattice parameter that is equal [case (b)] or very near [case (a)] to the parameter of sample S2. Thus, sample S1 contains KCN-rich grains without being inhomogeneous, neither on the macroscopic nor on the microscopic scale. This is just the situation of embedded nanocrystals which produce inhomogeneities on the submicroscopic scale. We conclude that the splitting of S1 reflections is a consequence of a strong nanocrystal-matrix interaction by a common cation sublattice.

Recently a model has been developed which describes the strain S_i and the stress T_i produced by nanocrystals embedded with low concentration in a crystalline matrix.¹⁴ It is based on the elastic continuum theory in the isotropic approximation. This is the standard treatment of the problem together with the adoption of appropriate geometrical conditions.^{1,21} We assume that the condition of low concentration holds in the sample S1. The sample is divided into spherical elastic domains. The average radius of the model unit is R_b and in its center the nanocrystal of radius R_0 is positioned. R_b is considered to be an effective radius which depends on the supersaturation $\Delta x = x - x_{ss}^a$ of the sample

$$(R_0/R_b)^3 = \Delta x. \quad (2)$$

With this definition a model unit with averaged radii R_0 and R_b should reflect the properties of the whole sample. However, the elastic conditions at the boundary of a domain are different for domains near to the surface of the sample and for domains in the central part of the sample. With increasing distance from the sample surface the conditions change from a free to a clamped boundary. In detail this effect depends on the quality of the crystal and on the size distribution and the relative positions of elastic domains.

B. Elastic domains

The center of the spherical model unit coincides with the origin of the spherical coordinates r, Θ, Φ . The lattice misfit

between nanocrystal and matrix is responsible for the interfacial gap ΔR between both materials which only appears without any relaxation processes. If interfacial forces exist, they close the gap by the radial displacements^{22,14}

$$u_r = ar + \frac{b}{r^2}, \quad (3)$$

where a and b are parameters which are determined by boundary conditions. Displacements are easily transferred into strains S_i and stresses T_i which are written by use of the condensed matrix notation as

$$S_r = \frac{\partial u_r}{\partial r} = a - 2\frac{b}{r^3} \quad \text{and} \quad S_\Theta = S_\Phi = \frac{u_r}{r} = a + \frac{b}{r^3},$$

$$T_r = C_{01}a - 2(c_{11} - c_{12})\frac{b}{r^3} \quad \text{and}$$

$$T_\Theta = T_\Phi = C_{01}a + (c_{11} - c_{12})\frac{b}{r^3}. \quad (4)$$

Here c_{ij} are elastic stiffness constants and $C_{01}=c_{rr}+2c_{r\Theta} = c_{11}+2c_{12}$ is one of the two scalar invariants of the elastic tensor.²³ In the present problem the three independent parameters a^{NC} , a^M , and b^M exist, where superscripts are referred to nanocrystal and matrix, respectively. a^{NC} and b^M/R_0^3 are expressed in terms of c_{ij} , $\Delta R/R_0$, and a^M by combining Eqs. (4) with the two boundary conditions

$$T_{r,0}^{NC} = T_{r,0}^M \quad \text{and} \quad u_{r,0}^{NC} - u_{r,0}^M = \Delta R \quad (5)$$

at $r=R_b$.

In the case of free domains the third condition $T_{r,b}=0$ at $r=R_b$ is used which is identical to the minimization of the deformation energy. The strain invariant $S_0^M = (S_r + S_\Theta + S_\Phi)/3$ is given by

$$S_0^M = a^M = \frac{-NC_{01}^{NC} \frac{\Delta R}{R_0} \left(\frac{R_0}{R_b}\right)^3}{C_{01}^M + N(C_{01}^{NC} - C_{01}^M) \left(\frac{R_0}{R_b}\right)^3}, \quad (6)$$

where $N=2(c_{11}-c_{12})^M/[C_{01}^{NC}+2(c_{11}-c_{12})^M]$. In the case of clamped domains the radial displacements vanish at $r=R_b$ which results in

$$S_0^M = a^M = \frac{C_{01}^{NC} \frac{\Delta R}{R_0} \left(\frac{R_0}{R_b}\right)^3}{C_{01}^{NC} + 2(c_{11} - c_{12})^M + (C_{01}^M - C_{01}^{NC}) \left(\frac{R_0}{R_b}\right)^3}. \quad (7)$$

C. Combining experimental results and the theoretical model

All changes of the material observed in several periods after crystal growth are consistent with phenomena one expects in the course of phase separation of a regular mixture. In this case all samples—including S1—on the upper horizontal line of Fig. 1 consist of two different crystalline com-

ponents. The nanocrystals in sample S1 are well separated which permits the use of the elastic continuum theory in its basic form.²² Thus, apart from the problem related to the detection of strains, the conditions with this kind of material are as simple as possible which gives some confidence that fundamental errors in analyzing the experimental results are avoided.

As only radial displacements appear around each nanocrystal and as there is no indication of optical birefringence in sample S1, there is neither a theoretical nor an experimental reason to assume that the observed splitting of Bragg reflections in S1 is caused by crystallographic anisotropy. Instead, we have to postulate two types of domains as the origin of splitting. The explanation of their appearance is slightly different for the two cases (a) and (b) mentioned at the end of Sec. III.

According to model (a) the broad subpeaks in Fig. 3 should be assigned to elastic domains without strong interfacial forces. This may happen if the continuity of the cation sublattice between both components is broken which is expected mainly for rather large grains. In this case the strain $S_0^{(\alpha)} = -8.4 \times 10^{-4}$ is described by Eq. (6). Using the maximal value $\Delta R/R_0 = 0.072$ and listed elastic constants²⁴ we determine $(R_0/R_b)^3 = \Delta x^{(\alpha)} = 0.019(5)$.

The strains $S_0^{(\beta+)}$ and $S_0^{(\beta-)}$ of model (b) are given by Eqs. (7) and (6). We again calculate the supersaturation and obtain $\Delta x^{(\beta+)} = 0.0072$ and $\Delta x^{(\beta-)} = 0.013$ which results in the average value $\Delta x^{(\beta)} = 0.010(3)$.

The values of $\Delta x^{(\alpha)}$ and $\Delta x^{(\beta)}$ have to be compared with those obtained by methods that analyze the chemical composition. Previously, the mole fractions x of solid solutions were determined by chemical analysis (potentiometric titration with a solution of $n/20$ AgNO₃) and by determining the density of as-grown crystals by the buoyancy method.¹⁶ There was no systematic difference between both kinds of results and the average relative error was less than 3%. As shown in Fig. 1, the material S1 was part of the solid solutions in the previous study. Its density was determined as $\rho^{(1)} = 3.0762$ g/cm³. After finishing all x-ray measurements, $\rho^{(1)}$ has been redetermined by use of a gas-displacement pycnometer. The result is $\rho^{(1)} = 3.0763(13)$ g/cm³, where the given error also reflects variations for different parts of the as-grown crystal. Because of its nice reproducibility we use $\rho^{(1)}$ together with the lattice parameters $a_{S1}^{(\alpha)}$ and $a_{S1}^{(\beta)}$ given in Sec. III to determine the chemical composition. Finally, the supersaturation is calculated on basis of Eq. (1). The result is $\Delta x_{\text{chemcomp}}^{(\alpha)} = 0.015(2)$ and $\Delta x_{\text{chemcomp}}^{(\beta)} = 0.012(2)$ in the case of models (a) and (b), respectively. Within the experimental uncertainties, there is a satisfactory agreement between $\Delta x_{\text{chemcomp}}$ obtained by use of standard techniques and the supersaturation determined from the splitting of reflections on basis of the theoretical model of elastic nanocrystal-matrix interactions.

Finally, we study the stability of the result against a variation of the deconvolution procedure. A second deconvolution of S1 reflections has been performed by fitting Lorentzian functions instead of Gaussian functions which have been applied in the first procedure (Fig. 3). The averaged Θ values of both types of analysis have been used to calculated the

relevant quantities. The lattice parameters for the two models are $a_{S1}^{(\alpha)} = 7.0541(13)$ [7.0525] Å and $a_{S1}^{(\beta)} = 7.0508(5)$ [7.0509] Å, where the data obtained from pure Gauss fits are repeated in brackets for the sake of comparison. As only the data of $a_{S1}^{(\beta)}$ are the same for both procedures and as they agree with $a_{S2} = 7.0507$ Å, model (b) should be preferred. This conclusion is also supported by the values of supersaturation which are now equal for both types of strains: $\Delta x^{(\beta+)} = \Delta x^{(\beta-)} = 0.013(4)$. This value is also consistent with $\Delta \chi_{\text{chemcomp}} = 0.014$. Thus, a mixture of Gaussian and Lorentzian curves even improves the internal consistency of the data. In conclusion, the agreement between both kinds of supersaturation shows that the elastic continuum theory works quantitatively in $(\text{KCN})_x(\text{KI})_{1-x}$.

V. CONCLUSION

The present work shows that elastic effects produced by embedded nanocrystals can be observed by measuring Bragg reflections of the matrix. A good resolution in diffraction experiments is needed to detect a splitting of reflections, it is necessary to determine the exact position of the sample in the phase diagram, and nucleation must be manageable in such a way that two different states of elastic deformations appear. These conditions are most easily realized in the case of a small concentration of nanocrystals which, in turn, favors the application of the elastic continuum theory. The agreement between theoretical description and experimental results supports the given interpretation of observed phenomena and indicates the general importance of the used model of elastic interactions.

In contrast to our results in $(\text{KCN})_x(\text{KI})_{1-x}$, the CuCl nanocrystals of $(\text{CuCl})_x(\text{NaCl})_{1-x}$ produce elastic deformations which are significantly larger than predicted by the elastic continuum theory.¹⁴ Apart from the piezoelectricity of CuCl both systems are very similar and interfacial forces originating in piezoelectric properties are not included in the elastic theory. We conclude that such forces are responsible for enhanced nanocrystal-matrix interactions in $(\text{CuCl})_x(\text{NaCl})_{1-x}$. This result is important for an improved treatment of nanocrystal structures containing piezoelectric components^{4,11,21} and in a more general sense it points out the importance of the chemical bonds acting between a nanocrystal and its environment.

ACKNOWLEDGMENTS

M. P. acknowledges the financial support by the *Graduiertenkolleg Struktur-Dynamik-Beziehungen in Mikrostrukturierten Systemen* at the University of Dortmund. C. S. and M. P. would like to thank M. Hess for his work during the commissioning of the preliminary diffraction setup and M. Volmer for his assistance at beam line SAW2. The authors would like to thank M. Tolan and kindly acknowledge the technical support of the DELTA staff.

- ¹V. A. Shchukin and D. Bimberg, *Rev. Mod. Phys.* **71**, 1125 (1999). C. Teichert, *Phys. Rep.* **365**, 335 (2002).
- ²U. Woggon, *Optical Properties of Semiconductor Quantum Dots*, Vol. 136 of Springer Tracts in Modern Physics (Springer, Berlin, 1997).
- ³B. Croset, Y. Girard, G. Prévot, M. Sotto, Y. Garreau, R. Pinchaux, and M. Sauvage-Simkin, *Phys. Rev. Lett.* **88**, 056103 (2002).
- ⁴I. Kegel, T. H. Metzger, A. Lorke, J. Peisl, J. Stangl, G. Bauer, J. M. Garcia, and P. M. Petroff, *Phys. Rev. Lett.* **85**, 1694 (2000).
- ⁵T. U. Schüllli, J. Stangl, Z. Zhong, R. T. Lechner, M. Sztucki, T. H. Metzger, and G. Bauer, *Phys. Rev. Lett.* **90**, 066105 (2003).
- ⁶A. Malachias, S. Kycia, G. Medeiros-Ribeiro, R. Magalhães-Paniago, T. I. Kamins, and R. S. Williams, *Phys. Rev. Lett.* **91**, 176101 (2003).
- ⁷A. I. Frenkel, A. V. Kolobov, I. K. Robinson, J. O. Cross, Y. Maeda, and C. E. Bouldin, *Phys. Rev. Lett.* **89**, 285503 (2002).
- ⁸R. Birringer, M. Hoffmann, and P. Zimmer, *Phys. Rev. Lett.* **88**, 206104 (2002).
- ⁹W. Vogel, S. Botti, S. Martelli, and E. Carlino, *New J. Chem.* **22**, 749 (1998).
- ¹⁰B. Palosz, E. Grzanka, S. Gierlotka, S. Stel'makh, U. Bismayer, J. Neufeind, H.-P. Weber, Th. Proffen, R. Von Dreele, and W. Palosz, *Z. Kristallogr.* **217**, 497 (2002).
- ¹¹S. Stel'makh, S. Gierlotka, E. Grzanka, H.-P. Weber, and B. Palosz, *J. Alloys Compd.* **382**, 138 (2004).
- ¹²S. Tsunekawa, K. Ishikawa, Z.-Q. Li, Y. Kawazoe, and A. Kasuya, *Phys. Rev. Lett.* **85**, 3440 (2000). V. Perebeinos, S.-W. Chan, and F. Zhang, *Solid State Commun.* **123**, 295 (2002).
- ¹³H. Fu and L. Bellaïche, *Phys. Rev. Lett.* **91**, 257601 (2003); T. Otto, S. Grafström, H. Chaib, and L. M. Eng, *Appl. Phys. Lett.* **84**, 1168 (2004); J.-H. Li, L. Chen, V. Nagarajan, R. Ramesh, and A. L. Roytburd, *ibid.* **84**, 2626 (2004).
- ¹⁴H.-J. Weber, J. Schreuer, and C. Popa-Varga, *Phys. Rev. B* **69**, 235419 (2004).
- ¹⁵W. Pies and A. Weiss, *Crystal Structure Data of Inorganic Compounds*, edited by K.-H. Hellwege, Landolt-Börnstein, New Series III/7 (Springer, Berlin, 1973).
- ¹⁶H.-J. Weber and H.-L. Keller, *Mater. Res. Bull.* **36**, 1777 (2001).
- ¹⁷R. D. Shannon, *Acta Crystallogr., Sect. A: Cryst. Phys., Diffr., Theor. Gen. Crystallogr.* **32**, 751 (1976); J. Ziolkowski, *J. Solid State Chem.* **57**, 269 (1985).
- ¹⁸D. Fröhlich, M. Haselhoff, K. Reimann, and T. Itoh, *Solid State Commun.* **94**, 189 (1995).
- ¹⁹M. Rossinelli, M. Bösch, and G. Zumofen, *Phys. Rev. B* **22**, 6403 (1980).
- ²⁰A. J. Cohen and G. G. Sumner, *Am. Mineral.* **43**, 58 (1958).
- ²¹V. A. Shchukin, D. Bimberg, T. P. Munt, and D. E. Jesson, *Phys. Rev. Lett.* **90**, 076102 (2003).
- ²²L. D. Landau and E. M. Lifschitz, *Theory of Elasticity* (Pergamon, New York, 1970).
- ²³J. Jerphagnon, D. Chemla, and R. Bonneville, *Adv. Phys.* **27**, 609 (1978).
- ²⁴A. G. Every and A. K. McCurey, *Second and Higher Order Elastic Constants*, edited by D. F. Nelson, Landolt-Börnstein, New Series III/29a (Springer, Berlin, 1992).